Universality and Intermittency of Pair Dispersion in Turbulence

Shiyong Tan and Rui Ni[*]

Department of Mechanical Engineering, The Johns Hopkins University, Baltimore, Maryland 21218, USA

Turbulence can disperse a concentrated parcel of pollutants at a rate over nine orders of magnitude higher than its purely diffusive counterpart. One intriguing signature of turbulent dispersion is its superdiffusive scaling. However, the universality of this scaling law is still in question. By leveraging a new laboratory facility, particle pairs with small initial separations can be tracked over four decades of separation in time and five decades of separation in squared displacement, thereby observing the full range of dispersion scaling laws. The results show that the classical Richardson cubic scaling will be reached not for an initial separation asymptotically close to zero but at a critical value, and this value does not appear to depend on the Reynolds number, providing an effective way to study universal dispersion dynamics. Additionally, the results agree well with the prediction based on the multifractal model and may help reconcile different reported scaling laws from laboratory experiments and field studies.

From the spread of virus-borne aerosols [1] to the transport of Fukushima-derived radioactive materials in the atmosphere [2], objects separating over several orders of magnitude in distance reveal the underlying mixing and transport dynamics of turbulence. To separate turbulent diffusion from the mean flow effect, pair dispersion, defined as the relative separation ($r(\tau) = |\mathbf{X}_2(\tau) - \mathbf{X}_1(\tau)|$) of two particles at respective positions of $\mathbf{X}_1(\tau)$ and $\mathbf{X}_2(\tau)$ at time τ, has become an important quantity to describe the turbulent transport and mixing.

The mean squared displacement $\langle (r(\tau) - r_0)^2 \rangle$ of particle pairs with separation growing from r_0 to r over a time interval of τ exhibits three distinct scaling laws, including the ballistic regime, Richardson superdiffusive regime [3], and the final diffusive regime [4–7]. The separation of two particles in the first ballistic range is simply driven by the initial velocity difference between the pairs. The superdiffusive dispersion occurs after $t_0 = \epsilon^{-1/3} r_0^{2/3}$, when the memory of the initial separation (r_0) is presumed to be forgotten and the dispersion only depends on τ and the turbulent energy dissipation rate ϵ following $\langle (r(\tau) - r_0)^2 \rangle = g\epsilon\tau^3$ with g being a universal constant. An important underlying assumption is that, as the Taylor-scale Reynolds number ($\mathrm{Re}_\lambda = u'\lambda/\nu$, where u' is the root-mean-squared fluctuation velocity, the Taylor microscale λ is $\sqrt{15\nu/\epsilon}u'$, and ν is the kinematic viscosity of the fluid) approaches infinity and r_0 becomes infinitesimal, this range expands and eventually dominates the entire dispersion behavior. But, so far it remains uncertain if any geophysical flows have ever reached a large enough Re_λ or if the effect of initial separation can really be ignored.

Laboratory experiments may provide a controlled environment to study the pair dispersion problem, but resolving the cubic scaling is very challenging because it requires the following conditions: $t_c \leq t_0 \ll T_L \leq t_R$ and $l_c \leq r_0 \ll L \leq l_R$, where t_c and l_c are the smallest timescale and length scale that a camera can resolve, respectively. T_L and L are the integral timescale and length scale, respectively. t_R is the residence time for particle pairs to remain in the view volume of size l_R.

To satisfy all these criteria, instead of increasing L as one would normally do to reach a large Re_λ, we did the opposite, by compressing the flow scales, t_c and l_c, via a system specifically designed to raise the mean energy dissipation rate $\langle \epsilon \rangle$. In practice, a vertical water tunnel (V-ONSET) was constructed (for details, see Supplemental Material [8] and Ref. [9]). The tunnel was powered by a jet array. By increasing the jet speed to over 12 m/s, the highest Reynolds number and energy dissipation rate that can be reached are $\mathrm{Re}_\lambda = 435$ and $\langle \epsilon \rangle = 0.16$ m²/s³, respectively. Compared with most previous experiments [13–15], the energy dissipation rate in our experiments was a few orders of magnitude larger. As a result, the Kolmogorov time ($\tau_\eta = 0.0035$ s) and length scales ($\eta = 55.8$ μm) are much smaller, and the turbulence is close to homogeneous and isotropic.

By combining the V-ONSET and our in-house dense particle tracking algorithm, OpenLPT [16], we satisfied the aforementioned criteria of both temporal and spatial scale separation. Of these two, the most stringent condition is temporal scale separation. Compared with previous experiments, i.e., $t_R/t_0 = 0.2$ [17], 2 [15], 7 [14], 13 [13], our experiment reached $t_R/t_0 = 76$, which is just barely enough for observing the Richardson scaling and for investigating its universality and the finite-Re_λ effect.

Once many long particle tracks are obtained from OpenLPT, particle pairs with a given initial separation r_0

were selected to calculate $\langle(r(\tau)-r_0)^2\rangle$. Figure 1 shows $\langle(r(\tau)-r_0)^2\rangle$ as a function of τ. Solid lines with different colors indicate different initial pair separations. Once the mean squared displacement is normalized by the longitudinal component $D_{LL}(r_0)$ of the Eulerian second-order structure function $S_2(r_0)=\langle(\mathbf{u}(\mathbf{r}+\mathbf{r}_0)-\mathbf{u}(\mathbf{r}))^2\rangle$ and τ is normalized by t_0, all solid lines collapse with one another for small τ because $D_{LL}(r_0)$ correctly accounts for the ballistic separation velocity between pairs of particles at early times.

The data covers roughly four decades of τ with about three decades below and one above t_0. For τ larger than t_0, the dispersion of particle pairs with small r_0 clearly exhibits a scaling that deviates from that in the ballistic ($\sim\tau^2$) or the diffusive range ($\sim\tau^1$). The scaling exponent k_D is not a constant; it has two limits, with k_D close to 3 for small r_0 (the Richardson scaling) and 1 for large r_0 (diffusive). Between these two limits, k_D decreases as r_0 increases. For the smallest initial separation $r_0\approx 0\sim 5\eta$ (red solid line), the superdiffusive scaling can be expressed as $\langle(r(\tau)-r_0)^2\rangle = g\epsilon\tau^3$, with g being the Richardson constant. g is believed to be a key universal constant of turbulence. Here, by fitting our data, this number is shown to be $g=0.542\pm 0.003$, which is close to the value previously reported from simulations [18].

The same particle pairs can also be utilized to calculate the Lagrangian relative velocity, i.e., $\delta_{r_0}\mathbf{v}(\tau)=\mathbf{u}(\mathbf{X}_2(\tau),\tau)-\mathbf{u}(\mathbf{X}_1(\tau),\tau)$. The Fig. 1 inset shows the evolution of $\langle\delta_{r_0}v^2(\tau)\rangle$ normalized by $S_2(r_0)$. At early times, solid lines with different initial separations all approach one because $\delta_{r_0}v^2(\tau)$ at $\tau=0$ recovers the limit of the
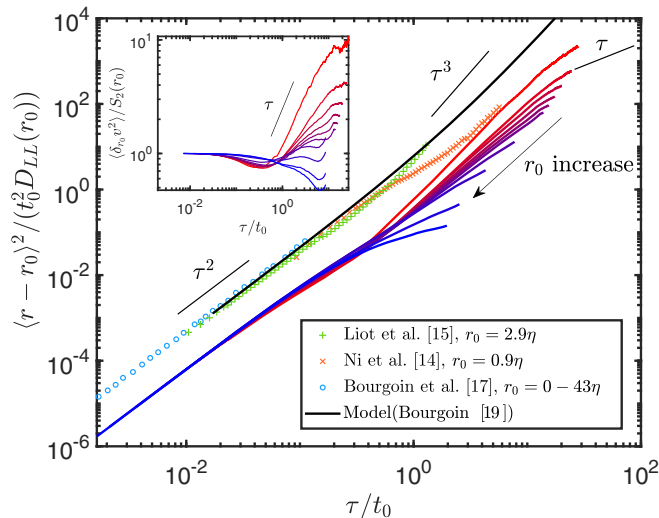

FIG. 1. Relative pair separation $\langle(r-r_0)^2\rangle$ for $r_0=0$–5η, 5–10η, 10–15η, 15–20η, 20–25η, 25–30η, 45–50η, 95–100η, 195–200η, 295–300η, with the color of the increasing r_0 gradually changing from red to blue. All previous results have been shifted up by one decade for clarity; Inset: $\langle\delta_{r_0}v^2\rangle$ compensated by the second-order structure function $S_2(r_0)$.

Eulerian second-order structure function $S_2(r_0)$. After $\tau=t_0$, different curves exhibit different scaling laws with the scaling exponent k_V clearly depending on r_0. For pairs with $r_0=0$–5η (red line), k_V is close to 1, i.e., $\langle\delta_{r_0}v^2(\tau)\rangle\propto\tau$, which is equivalent to the $\langle(r(\tau)-r_0)^2\rangle\propto\tau^3$ [4,20,21]. As r_0 increases, the scaling exponent k_V continues to drop in a manner similar to the trend of k_D.

To show the change of k_D with r_0 at different Re_λ, Fig. 2 compiles several different datasets. In addition to our experiments, including $\mathrm{Re}_\lambda=307$ and 450, we also expand the range of Re_λ by including other previous works using direct numerical simulations at $\mathrm{Re}_\lambda\approx 38$, 240 [18], 300 [22], 350 [18], 550 [23], and 700 [24]. All simulations were performed in homogeneous and isotropic turbulence similar to the conditions in our experiments, and the exponents were extracted by performing a simple least-square fit for the range of data between $2t_0\lesssim\tau\lesssim T_L/2$, with the error bars marking the 95% confidence interval of the fitted scaling exponent.

It is surprising to find that all datasets seem to intersect with one another at a critical initial separation of $r_{\mathrm{cr}}\approx 2$–4η, where k_D happens to be 3, i.e., Richardson's cubic scaling. For r_0 larger than r_{cr}, k_D drops very quickly and the rate of decay seems to depend on Re_λ and r_0. For r_0 smaller than r_{cr}, k_D clearly exceeds 3 instead of asymptotically approaching the Richardson's limit. Note that we did not include any data for $r_0<\eta$ [25,26] because pair separation in this regime grows exponentially instead of being governed by a power-law relationship.

To explain this observation, we provide a scaling transition model to understand the dependence of the exponent on the Reynolds number. We assume that, after the initial period of time that is dominated by a ballistic separation, the pair separation would enter a regime where the relative velocity between a pair of particles follows a power-law relationship with time: $\langle\delta_{r_0}v^2(\tau)\rangle/u'^2=(\tau/T_L)^{k_V}$ for $t_0<\tau<T_L$. Since the scale separation in time t_0/T_L can be easily converted to that in space r_0/L based on the relationship of $t=r/\delta_r u$, one can obtain $(\langle\delta_{r_0}v^2(t_0)\rangle/u'^2)^{1+k_V/2}=(r_0/L)^{k_V}$.

The relative velocity variance at t_0 is close to, but slightly smaller than, the initial relative velocity variance, i.e., $\langle\delta_{r_0}v^2(t_0)\rangle<\langle\delta_{r_0}v^2(0)\rangle$, which is displayed as the dip in Fig. 1 (inset). This phenomenon was also observed by Ouellette *et al.* [5], which was attributed to the effect of the negative mixed structure function [27]. To account for this effect, we introduce a constant γ so that $\delta_{r_0}v^2(t_0)=\gamma\delta_{r_0}v^2(0)$ ($\gamma<1$). By including two well-known relationships [$u'^2=(\epsilon L)^{2/3}$ [28] and $L/r_0=10^{-3/4}\mathrm{Re}_\lambda^{3/2}\eta/r_0$] and also recognizing that $\delta_{r_0}v^2(0)$ is the second-order Eulerian structure function by definition, we can express $(\gamma S_2(r_0)/(\epsilon L)^{2/3})^{1+k_V/2}=(10^{3/4}\mathrm{Re}_\lambda^{-3/2}r_0/\eta)^{k_V}$, which yields a clear relationship between k_V and the Taylor-scale Reynolds number.

The structure function $S_2(r_0)$ can be explicitly expressed following the Kolmogorov theory [29], $S_2(r_0) = \epsilon r_0^2/(3\nu)$ $(r_0 < r_*)$ or $11C_2(\epsilon r_0)^{2/3}/3$ $(r_0 > r_*)$, where $r_* = (11C_2)^{3/4}(\nu^3/\epsilon)^{1/4} = 10.6\eta$ is the transition length scale between the dissipative and inertial ranges, and C_2 is the Kolmogorov constant, which equals to 2.1. Given the relationship between k_D and k_V, i.e., $k_D = k_V + 2$ [4,20,21], we can predict the scaling exponent for pair dispersion with different initial pair separations. For $r_0 < r_*$, it follows

$$k_D = 3 + \frac{1.5\log(3/\gamma) - 2\log(r_0/\eta)}{\log \mathrm{Re}_\lambda - 0.5\log(3/\gamma) - 1}, \qquad (1)$$

while, for $r_0 > r_*$, the expression becomes

$$k_D = 3 - \frac{1.5\log(11C_2\gamma/3)}{\log\mathrm{Re}_\lambda - 0.67\log(r_0/\eta) + 0.5\log(11C_2\gamma/3) - 1}. \qquad (2)$$

Richardson's cubic scaling can be reached only if the second term in both Eqs. (1) and (2) is zero. For Eq. (1), this can be accomplished when either $\mathrm{Re}_\lambda \to \infty$ or the numerator becomes 0, which requires $r_0 = (3/\gamma)^{3/4}\eta$. γ can be estimated from the dip in Fig. 1 (inset), which is roughly 0.7. Although whether this number remains the same for other Reynolds numbers requires further investigations, here we assume that it is a constant. Finally, the Richardson scaling can be reached at the critical initial separation of $r_{\mathrm{cr}} = 3.0\eta$. For Eq. (2) in the inertial range, k_D can never reach 3 for a finite Re_λ because $\log(11C_2\gamma/3)$ is always larger than 0. This suggests that the finite Re_λ effect may always be present in the superdiffusive scaling of pair dispersion if r_0 is in the inertial range.

In Fig. 2, the predicted scaling exponent k_D is shown for different Re_λ ranging from 38 to 3×10^5. The model seems to agree both with our experiments and with previous simulations for the range of Re_λ considered. It can be clearly seen that the model lines consist of two different regimes. As r_0 increases, k_D decreases first linearly with $\log(r_0)$, following Eq. (1), and then nonlinearly with $1/\log(r_0)$, following Eq. (2). Although the model predicts that k_D approaches 3 for all r_0 when $\mathrm{Re}_\lambda \to \infty$, it is in fact a slow process because $k_D \propto 3 - 1/\log(\mathrm{Re}_\lambda)$. Therefore, even for a Reynolds number at $\mathrm{Re}_\lambda = 10^5$ that is beyond what most natural flows can reach, the effect of the initial separation is still very important.

Furthermore, the intersection of all curves at $r_{\mathrm{cr}}/\eta = 3.0$, where k_D recovers Richardson's cubic scaling, implies that the dispersion statistics at r_{cr} is free from the Reynolds number effect. This r_{cr} provides a valuable way to peek into the asymptotic dispersion statistics at the limit of the infinite Reynolds number. In particular, we examine the distribution of the pair separation $\Delta r = r(\tau) - r_0$ at different time delays τ, $p(\Delta r, \tau)$. It was suggested by Richardson that $p(\Delta r, \tau)$ should follow the functional form of
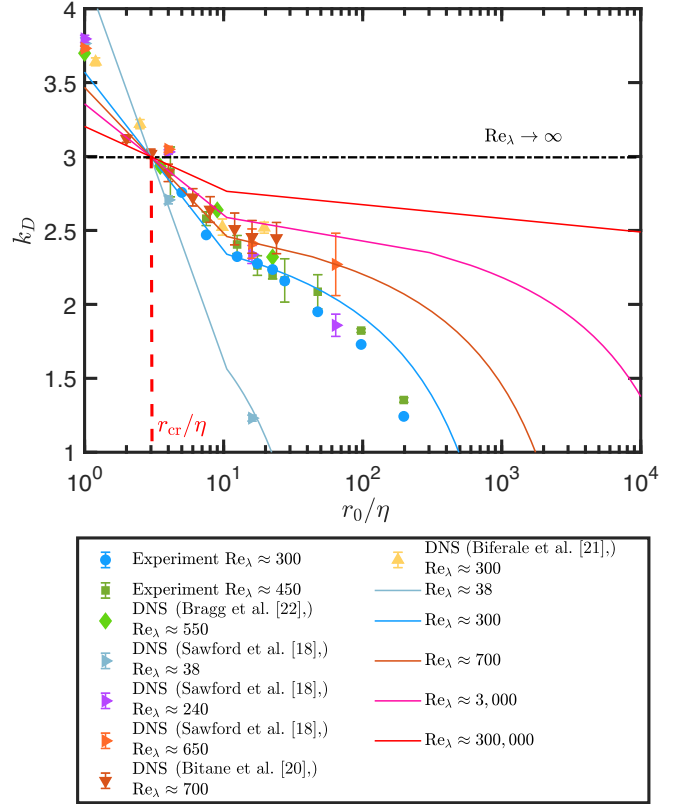

FIG. 2. The dependence of the superdiffusive dispersion scaling exponent k_D on the initial particle separation r_0. Solid lines represent model predictions for different Reynolds numbers calculated from the model described by Eqs. (1) and (2). The dashed red line shows the intersection point at $r_{\mathrm{cr}}/\eta = 3$ for all Reynolds numbers, and the dash-dotted black line indicates the model prediction for $\mathrm{Re}_\lambda \to \infty$.

$-\beta\exp(\Delta r^\alpha)$, and $\alpha = 2/3$ was predicted based on the experimental observation [3]. However, since then, different values of α and shapes of probability density functions (PDF) have been proposed, including 2/3 [13], 0.5 [30–32], and a variable depending on τ [24,33].

Our experiments suggest that $p(\Delta r, \tau)$ and α are sensitive to both r_0 and τ. The various α reported previously could be a result of the different r_0 values used. Since the statistics for r_0 around 3η does not depend on Re_λ, we show the normalized $p(\Delta r, \tau)$ for the same initial separation $r_0 = 0$–5η at five different time delays τ. These τ are selected so they are in the range ($t_0 < \tau < T_L$) where the Richardson's cubic scaling law is observed. The measured $p(\Delta r, \tau)$ is fitted with $-\beta\exp(\Delta r^\alpha)$, and the obtained α is shown as a function of τ/t_0 in the inset, which exhibits a clear linear relationship with τ from the Richardson-predicted exponent, $\alpha = 2/3$, to the Gaussian-like exponent, $\alpha = 2$.

Since a smaller α indicates a PDF with a longer tail, the results suggest that events of pairs separating much faster than average occur more frequently at early times (small τ), which is a signature of intermittency in turbulence. To evaluate this dispersion intermittency, the high-order

statistics $\langle \Delta r^p \rangle = \int_0^\infty r^p p(r,\tau) dr \sim \tau^{\zeta_p}$ is calculated, where ζ_p is the exponent of dispersion for the order p.

If dispersion in turbulence is not affected by intermittency, by assuming that the superdiffusive regime only depends on ϵ and the time delay τ, one can easily obtain $\langle \Delta r^p \rangle \sim (\epsilon \tau^3)^{p/2}$ with $\zeta_p = 3p/2$. For $p = 2$, ζ_2 equals three, which agrees with the Richardson cubic scaling. For higher orders, ζ_p/ζ_2 increases linearly with p, which is shown as the black solid line in Fig. 3(b). ζ_p can also be calculated from $\langle r^p \rangle = \int_0^\infty -\beta r^p \exp(r^\alpha) dr$. If we set α and β as fixed constants, as suggested by Richardson, the scaling exponents are shown as blue diamonds, which coincide with the black solid line, because constants α and β indicate that the separation PDF remains unchanged at different scales with no intermittency.
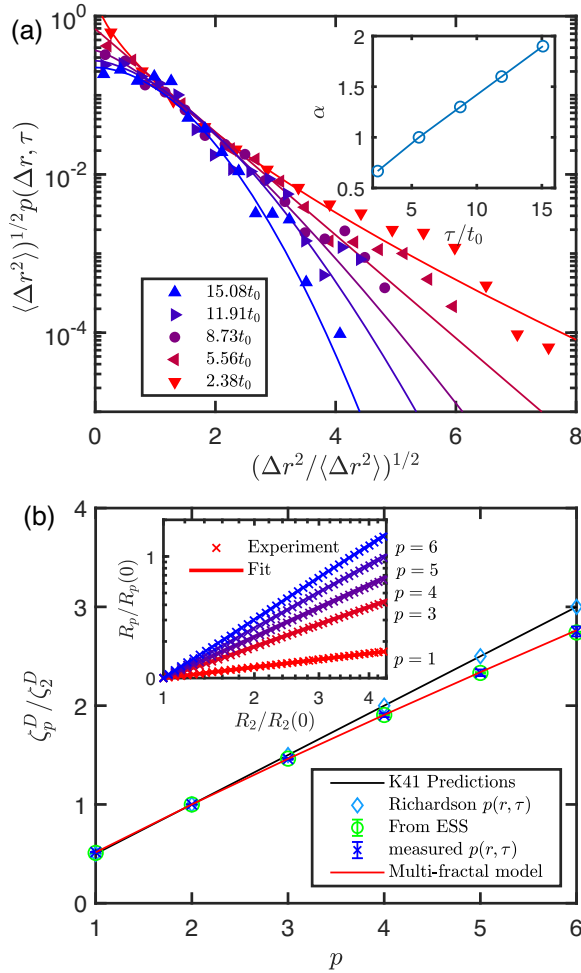

FIG. 3. (a) The probability density function of the normalized particle separation $(\Delta r^2/\langle \Delta r^2 \rangle)^{1/2}$ for constant initial separation $r_0 = 0$–5η at different τ. The symbols represent experimental measurements, and solid lines of the same respective color indicate the fit to the function of $p(\Delta r, t) = -\beta \exp(\Delta r^\alpha)$. (b) The exponent of pair dispersion, ζ_p^D, with respect to p; Inset: the ESS plot of the higher-order statistics of the pair separation $R_p = \langle (r - r_0)^p \rangle$ against the second order.

Experimentally, the scaling exponent ζ_p can be extracted directly from experiments by plotting the higher-order pair dispersion ($\langle \Delta r^p \rangle$) against the second-order one ($\langle \Delta r^2 \rangle$) using the extended self similarity (ESS) method [34], as shown in Fig. 3(b) inset. The extracted exponents ζ_p for p ranging from 2 to 6 are shown as the green symbols in Fig. 3(b). In addition to this direct measurement, $\langle \Delta r^p \rangle$ can also be estimated from the measured $p(r,\tau)$ in Fig. 3(a) following $\langle \Delta r^p \rangle = \int_0^\infty r^p p(r,\tau) dr$, which provides an indirect way to estimate the exponent ζ_p. The results are plotted in Fig. 3(b) as blue symbols.

It is clear that, as p increases, both directly and indirectly measured ζ_p systematically deviate from Richardson's prediction. The deviation is not as strong as that in the Eulerian [35] and Lagrangian structure functions [36,37] because pair dispersion is integrated from the velocity increment, which tends to smooth out intermittent events. Nevertheless, the deviation is still a clear indication of turbulence intermittency in pair dispersion. This finding is consistent with the aforementioned scale-dependent $p(\Delta r, \tau)$.

To further confirm the observed intermittency, we decide to model ζ_p using the multifractal framework [38], which starts with a relationship between the velocity increment $\delta u(r)$ at a separation of r: $\delta u(r) \sim (r/L)^h$ (h is the fractal dimension). Since the eddy turnover time $\tau \sim r/\delta u(r)$, it yields $r \sim \tau^{1/(1-h)}$. Based on this, the higher order of r can be expressed as $\langle r^p \rangle \sim \int_{h \in I} dh \tau^{(p+3-D(h))/(1-h)} \sim \tau^{\zeta_p^D}$, where $D(h)$ characterizes the hierarchy of fractal dimensions that are associated with different intermittency levels. Based on this equation, the scaling exponent ζ_p^D can be obtained following

$$\zeta_p^D = \inf_h \left(\frac{p + 3 - D(h)}{1 - h} \right). \qquad (3)$$

If pair dispersion is subjected to similar turbulence intermittency as in the Eulerian framework, they should share the same hierarchy of fractal dimensions, i.e., $D(h)$. For the Eulerian structure functions, $D(h)$ is directly related to the scaling exponent ζ_p^E, which must satisfy the exact relationship $\zeta_3^E = 1$ at $p = 3$. This requirement leads to $D(h) \leq 3h + 2$. Substituting this constraint into Eq. (3) shows that $\zeta_2^D = 3$, which is consistent with Richardson's prediction. For other orders, we can determine $D(h)$ from the Legendre transform $\zeta_p^E = \inf_h(ph - D(h) + 3)$ [38]. Repeating the same procedure results in a prediction for ζ_p^D, which is shown in Fig. 3(b) as a red solid line. This line overlaps perfectly with the experimental measurement and captures the deviation from Richardson's prediction due to intermittency.

Since $D(h)$ from the Eulerian structure function provides an excellent prediction for pair dispersion in the Lagrangian framework, it supports the argument that the dispersion

statistics for particle pairs at a critical separation r_{cr} successfully capture some universal characteristics of turbulence. The various previously reported scaling laws may be a result of the uncontrolled initial separations and different Reynolds numbers used.

In summary, our findings suggest that the Richardson scaling holds either for all initial pair separations at $Re_\lambda \to \infty$ or for nearly all finite Reynolds numbers at one critical initial separation $r_{cr} = 3\eta$. This r_{cr} represents the length scale, at which the inertial-range Lagrangian velocity scale separation can be directly and solely related to the temporal scale separation. This critical initial separation provides a valuable way for us to study dispersion intermittency. The results imply that pollutants concentrated in a small local region could potentially disperse and spread much faster than the mean. Therefore, future predictive models on transport and mixing should consider accounting for the intermittency, finite Reynolds number, and initial separations altogether.

---

*rui.ni@jhu.edu

[1] R. Mittal, R. Ni, and J.-H. Seo, The flow physics of COVID-19, J. Fluid Mach. **894** (2020).

[2] R. Mészáros, Á. Leelőssy, T. Kovács, and I. Lagzi, Predictability of the dispersion of Fukushima-derived radionuclides and their homogenization in the atmosphere, Sci. Rep. **6**, 19915 (2016).

[3] L. F. Richardson, Atmospheric diffusion shown on a distance-neighbour graph, Proc. R. Soc. A **110**, 709 (1926).

[4] G. Batchelor, The application of the similarity theory of turbulence to atmospheric diffusion, Q. J. R. Meteorol. Soc. **76**, 133 (1950).

[5] N. T. Ouellette, H. Xu, M. Bourgoin, and E. Bodenschatz, An experimental study of turbulent relative dispersion models, New J. Phys. **8**, 109 (2006).

[6] J. P. Salazar and L. R. Collins, Two-particle dispersion in isotropic turbulent flows, Annu. Rev. Fluid Mech. **41**, 405 (2009).

[7] F. Toschi and E. Bodenschatz, Lagrangian properties of particles in turbulence, Annu. Rev. Fluid Mech. **41**, 375 (2009).

[8] See Supplemental Material at http://link.aps.org/supplemental/10.1103/PhysRevLett.128.114502 for the details of experimental setup and turbulence information, which includes Refs. [9–12].

[9] A. U. M. Masuk, A. Salibindla, S. Tan, and R. Ni, V-ONSET (vertical octagonal noncorrosive stirred energetic turbulence): A vertical water tunnel with a large energy dissipation rate to study bubble/droplet deformation and breakup in strong turbulence, Rev. Sci. Instrum. **90**, 085105 (2019).

[10] S. Tan, A. Salibindla, A. U. M. Masuk, and R. Ni, Introducing openLPT: New method of removing ghost

[11] particles and high-concentration particle shadow tracking, Exp. Fluids **61**, 47 (2020).

[11] E. A. Variano, E. Bodenschatz, and E. A. Cowen, A random synthetic jet array driven turbulence tank, Exp. Fluids **37**, 613 (2004).

[12] E. A. Variano and E. A. Cowen, A random-jet-stirred turbulence tank, J. Fluid Mach. **604**, 1 (2008).

[13] S. Ott and J. Mann, An experimental investigation of the relative diffusion of particle pairs in three-dimensional turbulent flow, J. Fluid Mech. **422**, 207 (2000).

[14] R. Ni and K.-Q. Xia, Experimental investigation of pair dispersion with small initial separation in convective turbulent flows, Phys. Rev. E **87**, 063006 (2013).

[15] O. Liot, D. Martin-Calle, A. Gay, J. Salort, F. Chillà, and M. Bourgoin, Pair dispersion in inhomogeneous turbulent thermal convection, Phys. Rev. Fluids **4**, 094603 (2019).

[16] S. Tan, A. Salibindla, A. U. M. Masuk, and R. Ni, An open-source Shake-the-Box method and its performance evaluation, in *13th International Symposium on Particle Image Velocimetry, Munich, Germany* (2019).

[17] M. Bourgoin, N. T. Ouellette, H. Xu, J. Berg, and E. Bodenschatz, The role of pair dispersion in turbulent flow, Science **311**, 835 (2006).

[18] B. L. Sawford, P. Yeung, and J. F. Hackl, Reynolds number dependence of relative dispersion statistics in isotropic turbulence, Phys. Fluids **20**, 065111 (2008).

[19] M. Bourgoin, Turbulent pair dispersion as a ballistic cascade phenomenology, J. Fluid Mech. **772**, 678 (2015).

[20] M. P. Rast and J.-F. Pinton, Pair Dispersion in Turbulence: The Subdominant Role of Scaling, Phys. Rev. Lett. **107**, 214501 (2011).

[21] R. Bitane, H. Homann, and J. Bec, Time scales of turbulent relative dispersion, Phys. Rev. E **86**, 045302(R) (2012).

[22] L. Biferale, G. Boffetta, A. Celani, B. Devenish, A. Lanotte, and F. Toschi, Lagrangian statistics of particle pairs in homogeneous isotropic turbulence, Phys. Fluids **17**, 115101 (2005).

[23] A. D. Bragg, P. J. Ireland, and L. R. Collins, Forward and backward in time dispersion of fluid and inertial particles in isotropic turbulence, Phys. Fluids **28**, 013305 (2016).

[24] R. Bitane, H. Homann, and J. Bec, Geometry and violent events in turbulent pair dispersion, J. Turbul. **14**, 23 (2013).

[25] G. K. Batchelor, The effect of homogeneous turbulence on material lines and surfaces, Proc. R. Soc. A **213**, 349 (1952).

[26] A. Monin, A. Yaglom, and J. Lumley, Mechanics of turbulence, Stat. Fluid Mech. **2** (1975).

[27] K. Chang, B. J. Malec, and R. A. Shaw, Turbulent pair dispersion in the presence of gravity, New J. Phys. **17**, 033010 (2015).

[28] K. R. Sreenivasan, An update on the energy dissipation rate in isotropic turbulence, Phys. Fluids **10**, 528 (1998).

[29] A. Kolmogorov, The local structure of isotropic turbulence in an incompressible viscous fluid, Dokl. Akad. Nauk SSSR **30**, 301 (1941).

[30] M.-C. Jullien, J. Paret, and P. Tabeling, Richardson Pair Dispersion in Two-Dimensional Turbulence, Phys. Rev. Lett. **82**, 2872 (1999).

[31] I. M. Sokolov, J. Klafter, and A. Blumen, Ballistic versus diffusive pair dispersion in the Richardson regime, Phys. Rev. E **61**, 2717 (2000).

[32] F. Nicolleau and J. C. Vassilicos, Turbulent Pair Diffusion, Phys. Rev. Lett. **90**, 024503 (2003).

[33] R. Scatamacchia, L. Biferale, and F. Toschi, Extreme Events in the Dispersions of Two Neighboring Particles under the Influence of Fluid Turbulence, Phys. Rev. Lett. **109**, 144501 (2012).

[34] R. Benzi, S. Ciliberto, R. Tripiccione, C. Baudet, F. Massaioli, and S. Succi, Extended self-similarity in turbulent flows, Phys. Rev. E **48**, R29 (1993).

[35] F. Anselmet, Y. Gagne, E. Hopfinger, and R. Antonia, High-order velocity structure functions in turbulent shear flows, J. Fluid Mach. **140**, 63 (1984).

[36] L. Biferale, G. Boffetta, A. Celani, B. J. Devenish, A. Lanotte, and F. Toschi, Multifractal Statistics of Lagrangian Velocity and Acceleration in Turbulence, Phys. Rev. Lett. **93**, 064502 (2004).

[37] H. Xu, M. Bourgoin, N. T. Ouellette, and E. Bodenschatz, High Order Lagrangian Velocity Statistics in Turbulence, Phys. Rev. Lett. **96**, 024503 (2006).

[38] U. Frisch and A. N. Kolmogorov, *Turbulence: The Legacy of AN Kolmogorov* (Cambridge University Press, Cambridge, England, 1995).